WOOD RESEARCH doi.org/10.37763/wr.1336-4561/67.5.744759
e-ISSN 2729-8906
67(5): 2022 744-759 pp.

RESEARCH ON THE EFFECT OF WOOD SURFACE CRACKS ON PROPAGATION CHARACTERISTICS AND ENERGY ATTENUATION OF LONGITUDINAL ACOUSTIC EMISSION

CHANGLIN HUANG[1], MING LI[2], SAIYIN FANG[1], YUE ZHAO[1], FEILONG MAO[1], ZHOULING YANG[1], TINGTING DENG[1]

[1]SOUTHWEST FORESTRY UNIVERSITY
CHINA
[2]ANHUI POLYTECHNIC UNIVERSITY
CHINA

(RECEIVED APRIL 2022)

ABSTRACT

To investigate the effect of *Zelkova schneideriana* surface cracks on the longitudinal wave propagation characteristics of acoustic emission (AE). Different sizes and numbers of cracks were made on the surface of the specimen, the propagation characteristics of AE longitudinal waves along wood texture direction were studied. Firstly, five regular cracks with the same length, different width, depth and equidistant distribution were fabricated on the surface of the specimen. The burst and continuous AE sources were generated by lead core breakage and signal generator, and the AE signals were acquired by 5 sensors with sampling frequency was set to 500 kHz. Then, the propagation speed of AE longitudinal wave was calculated by Time Difference of Arrival (TDOA) based on lead core breakage. Finally, the 150 kHz pulse signals of different voltage levels generated by the signal generator were used as AE sources to study the influence of cracks on the attenuation of AE longitudinal wave energy. The results showed that the AE longitudinal wave propagation speed under the crack-free specimen was 4838.7 $m \cdot s^{-1}$. However, after the regular crack was artificially made, the longitudinal wave speed reduced to a certain extent, and the relative error of the change was not more than 9%. Compared with the energy decay rate of 1.29 in the crack-free specimen, the decay rate gradually increased to 2.08 with the increase of the crack cross-sectional area.

KEYWORDS: *Zelkova schneideriana*, surface cracks, acoustic emission longitudinal waves, energy decay rate.

INTRODUCTION

In life, wood materials are often used as bearing members because of their lightweight, high ratio of strength to weight and good elasticity. The existence of cracks will affect its mechanical properties and reduce the use value of the wood, therefore, when the wood is used in real life, it is necessary to detect it, and to monitor the health of some in-service components to prevent safety accidents (Wang et al. 2020). As one of the non-destructive testing(NDT) technologies, acoustic emission technology (AE) has been widely used in the detection of metals, rocks and composites (Liu et al. 2018, Urbaha et al. 2021, Vinogradov and Merson. 2018). With the development of AE, it has gradually been used in the detection of wood, analyzing the AE signal characteristics of wood fracture (Lamy et al. 2015), monitoring the effect of wood moisture content (MC) changes on its properties (Bertolin et al. 2020), and changes in wood drying process (Kowalski et al. 2004). According to the theory of material mechanics and acoustic emission detection, when the material suffers damage, the local source energy will be released rapidly in the form of stress waves to achieve a low-energy stable state, this phenomenon is called acoustic emission (WU et al. 2014). This was discovered by Kaiser in the early 1950s when he studied metals with irreversible AE phenomena and later defined this irreversible AE phenomenon as the Kaiser effect, and in subsequent studies Kaiser also proposed the concept of burst and continuous AE signals.

The technology has also been gradually used to monitor wood damage, and the study of wood defects and damage has been a hot issue in the industry. Lukomski et al. (2017) used AE to monitor the micro-damage of wooden artifacts exposed to the air environments, showing that AE can directly reflect the physical changes caused by the environment, and explored the suitable environment which can be used in the conservation of wooden artifacts. Guo et al. (2019) used AE to study the fracture toughness of wood-plastic composites (WPC), and determined the critical load by the relationship between AE cumulative events and time and load, to calculate the critical stress intensity factor and fracture toughness, which showed that the fracture toughness of WPC increased with the increase of wood fiber content. Reiterer et al. (2002) used a wedge splitting test to explore the characteristics of wood type I fracture, and separately loaded hardwoods and softwoods in the vertical wood grain direction. The results showed that the crack propagation process of softwood was stable, and few micro cracks produced by hardwood in the crack initiation stage, which was closer to brittle fracture. Wood damage has both internal and surface damage; therefore, it is necessary to analyze the characteristics of AE signals on the surface and internal of wood to identify the types of wood damage and provide a reference for practical applications. Deng et al. (2021) and Ju et al. (2019) explored the propagation characteristics of AE signals on the wood surface, indicating the effect of wood anisotropy on AE signal propagation. Diakhate et al. (2017) used AE to monitor the internal crack extension of wood to further clarify the cracking mechanism of wood, which reduced the safety risk for practical engineering applications. Wood used as construction material is usually exposed to the external environment for a long time, and decay often occurs due to various fungi, resulting in a sharp decline in the mechanical properties of wood, therefore, Raczkowski et al. (1999) verified the damage of wood at the early stage of decay with the change of AE accumulation counts.

Wood is also processed into supporting beams, industrial plywood, particle boards, etc., which have been studied by scholars using AE to analyze the damage signals of wood materials in different states and to provide a basis for identifying damage types (Rescalvo et al. 2020, Ritschel et al. 2014, Vun et al. 2005).

When the material is damaged under the loading condition, there is the release of strain energy, to further clarify the energy release during material fracture. Xing et al. (2019) conducted cyclic loading tests on sandstone specimens and characterized the damage process of sandstone using AE energy analysis, and proposed a theoretical model of subcritical fracture extension characterized by the evolution of the fracture process zone (FPZ), and subcritical fracture process of sandstone agrees well with a theoretical model. Azadi et al. (2021) analyzed the energy and cumulative energy of the AE signal under cyclic loading, indicating that the AE energy can effectively characterize the damage fracture process of the material. Therefore, the study of AE energy changes in wood has become a hot issue, whereas, in the current study, mostly researchers use lead core fracture as an AE source to simulate the damage of the material, and clarify the propagation characteristics of AE signals generated by simulated damage sources, thus providing a theoretical reference for the study of AE source localization (Dong et al. 2020, Sause 2011). Wang et al. (2021) used lead core fracture to simulate wood damage and compared it to the real wood fracture, it was shown that lead core fracture can effectively simulate wood's real damage, by analyzing the characteristics of the acquired AE signals. To study the attenuation changes of AE energy in wood, Ming et al. (2021) and Ding et al. (2022) designed experiments to acquire surface transverse and internal longitudinal waves of wood to investigate the propagation characteristics and energy attenuation characteristics of different AE signals in wood, and the two types of signals showed obvious differences in their speed and energy attenuation.

The absence of defects in the specimen is usually a basic prerequisite for existing studies on the subject. Wood defects, especially the development of cracks, can lead to a significant reduction in wood strength or even failure. Therefore, studying the effect of cracks on AE propagation processes is a fundamental problem that AE needs to address urgently in the field of wood NDT. In this study, regular cracks of different sizes and numbers were first sawn on the surface of wood specimens, and two types of AE signals were generated on the surface of the specimens by lead core fracture and signal generator, the latter of which was mainly used to study the decay law of AE energy. Then the AE signal waveforms of different crack sizes and numbers were used to calculate the AE longitudinal wave speed based on the TDOA method. Finally, a defined AE source was generated by the signal generator. According to the principle of Alternating Current (AC), the decay law of AE energy with the change of cracks was calculated and explored.

MATERIALS AND METHODS

Test materials and equipment

Zelkova schneideriana specimens with the surface defect-free size of 800 × 60 × 30 mm (length × width × height) were selected, the MC is about 12.2 %, density is 0.75 $g \cdot cm^{-3}$.

The experimental specimens were divided into 6 groups, and regular cracks were made on the surface of 5 groups. The specific size and distribution of cracks are shown in Fig. 1. The 6 groups of specimens are defined as specimen 1 to specimen 6 (T1~T6), and the specific parameters of the specimen cracks are shown in Tab. 1.

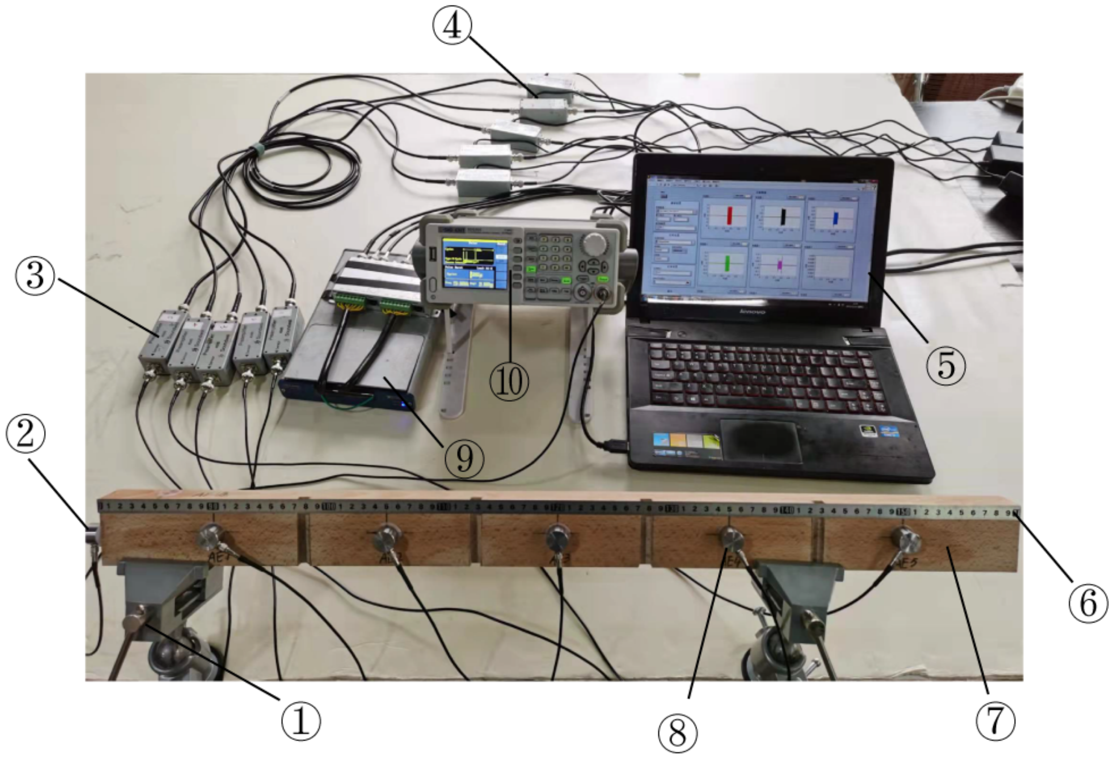

Fig. 1: Experiment diagram: 1- clamps, 2- AE source, 3- AE signal amplifier (40 dB), 4- AE signal splitter, 5- acquisition computer, 6- ruler, 7- Zelkova Schneideriana specimen, 8- AE sensors, 9- high-speed acquisition card (NI USB-6366), 10- single channel signal generator (SDG805).

To acquire the AE signals generated by the experiment, a 5-channel AE signal acquisition system was built with NI USB-6366 high-speed acquisition card and Lab VIEW2017 software. Its acquisition card voltage range was set to (-5V, 5V) with a maximum sampling frequency reaching 2 MHz at the same time, to ensure the stability of the AE signal transmission, it was equipped with a preamplifier with a gain of 40 dB to amplify the collected AE signal. The single-ended resonant RS-2A AE sensor had a frequency range of 50 kHz ~ 400 kHz. To ensure sufficient contact between the sensor and the specimen surface, high-temperature insulating silicone grease was used to fill between the sensor and the specimen. Li (2017) and Shen et al. (2015) showed that the maximum AE frequency of wood was about 200 kHz. According to the Nyquist sampling theorem (Fang et al. 2018, Dong and Li 2020), to recover the analog signal without distortion, the signal sampling frequency f_s and the maximum signal frequency f_{max} must satisfy $f_s \geq 2f_{max}$. Therefore, the sampling frequency was set to 500 kHz. In this experiment, the SIGLENT SDG805 single-channel signal generator was used to output pulse signal to simulate the damage signal of wood. The maximum output frequency is 5 MHz, the maximum sampling rate is 125 MSa·s^{-1}, and the output voltage range is 4 mVpp ~ 20 Vpp.

Tab.1: Crack parameters of specimens.

Specimen number	Specimen 1	Specimen 2	Specimen 3	Specimen 4	Specimen 5	Specimen 6
Crack sizes (width × depth) (mm)	0	6×4	6×6	6×8	8×8	10×8

Methods

The lead core breaking and signal generator were used as AE sources on the specimen surface to simulate the dynamic damage of wood, and Wang et al. (2021) showed that lead core fracture on the surface of wood specimens can better reflect its damage characteristics. The signal generated by lead core breakage was used to calculate the AE longitudinal speed, however, due to the short duration of the AE signal generated by lead core breakage. The standard pulse signal generated by the signal generator was used as the simulated AE source to calculate the AE longitudinal wave energy. According to the elastic wave theory, when the vibration direction of the wave generated by the AE source is the same as the propagation direction, the AE signal propagates mainly in the form of longitudinal wave. The longitudinal wave can propagate in any medium, and the energy will be decayed when it passes through different mediums. To clarify the propagation rate and energy attenuation of longitudinal waves in specimens with different crack sizes, the AE longitudinal wave extraction test was designed, as shown in Fig. 1. When calculating the AE longitudinal wave energy, the AE signal is regarded as an AC signal, and the heat generated through the unit resistance within a certain time is calculated as the energy of the AE signal.

As shown in Fig. 1, 4 cracks were made on the specimen with equal spacing on the surface, the crack spacing was 150 mm, and the outermost 2 cracks were 175 mm away from both end faces of the specimen, respectively. Each crack was taking as the center, and the AE sensors were placed at 75 mm between the left and right, to ensure that all AE sensors were in a common line. The sensors are S1~S5 from left to right, and the AE source was located on the left end face of the specimen, which was co-linear with the AE sensors. The AE longitudinal energy decay law of different voltage levels was studied by changing the intensity of the pulse signal, and the sensor position was not changed during the test. Meanwhile, to ensure the consistency of the AE source frequency, 150 kHz pulse signal was used, the single pulse width was 1μs, the cycle number was 15000, cycle period was 1s. In the lead core break test, the experimental process referred to the American ASTM-E976 standard, the 0.5 mm diameter lead core was placed at an angle of 30° with the surface of the specimen, and it was broken at 2.5 mm from the contact point, to obtain original AE signals.

According to the elastic wave theory (Ohtsu and Masayasu 2016, Liu and Khvesyuk 2020), the longitudinal wave propagates faster than the transverse wave, and the first to reach the sensor is the longitudinal wave (Ting 2006). The time difference Δt is calculated using the two-point time difference localization method, where the distance Δs between each sensor is fixed, then according to the speed formula $v= \Delta s/\Delta t$, the AE longitudinal wave propagation rate between the two sensors can be calculated. AE signal can be regarded as AC signal when analyzing AE energy attenuation. In the transmission process, there is a part of energy loss, and the heat generated by unit resistance within a certain time t is taken as the energy carried by the AE signal. As shown in Eq. 1:

$$W = \int_0^t \frac{U^2}{R} d\tau \tag{1}$$

where: U - Voltage, unit is V, R – Resistance, unit is Ω.

Since the AE signals collected by the system were discontinuous, Eq. 1 is discretized. The two data are separated by $1/f_s$ second, and if the discrete process uses a zero-order retainer, i.e., the signal amplitude remains constant during this time, then its energy is calculated by the Eq. 2:

$$W = \sum_{i=1}^{n} \Delta t \cdot u_i^2 = nT \sum_{i=1}^{n} u_i^2 \tag{2}$$

where: $\Delta t_i = T = 1/f_s$ $(i = 1,2,....,n)$, f_s - the sampling frequency, n - data length.

RESULTS AND ANALYSIS

Effect of cracks on AE longitudinal wave speed

The AE signal will form a relatively stable standing waveform after a short transition process. Based on the mechanical fluctuation theory, the longitudinal wave propagates faster than the transverse wave, and the first component to reach the sensor is mainly longitudinal wave. Therefore, TDOA is used to calculate the time difference (Aljets et al. 2012), to calculate the propagation speed of longitudinal wave. To clarify the effect of wood surface cracks on AE longitudinal speed, the effect of crack size and distribution on AE longitudinal speed was investigated using the longitudinal waves collected by each sensor. At the same time, to reduce the interference of human and environmental factors in the experimental process, 10 independent experiments were conducted for each group of specimens, respectively. where v_i is the propagation speed of the AE longitudinal wave in the wood specimen, and i (i = 1,2,3,4) is the number of cracks. The experimental results are shown in Tabs. 2, 3 and 4.

Tab. 2: Effect of crack distribution on AE longitudinal wave speed.

Experiment number	Specimen 1	Specimen 2			
	v (m·s^{-1})	v_1 (m·s^{-1})	v_2 (m·s^{-1})	v_3 (m·s^{-1})	v_4 (m·s^{-1})
1	4838.7	4891.3	4545.5	4787.2	4918.0
2	4838.7	4411.8	4545.5	4787.2	4918.0
3	4838.7	5000.0	4838.7	4687.5	4285.7
4	4838.7	4687.5	4545.5	4787.2	4918.0
5	4838.7	4687.5	4545.5	4787.2	4918.0
6	4838.7	4687.5	4545.5	4787.2	4918.0
7	4838.7	5000.0	4545.5	4591.8	4918.0
8	4838.7	5000.0	4545.5	4787.2	4918.0
9	4838.7	4891.3	4545.5	4687.5	4838.7
10	4838.7	4687.5	4545.5	4787.2	4285.7
Average value	4838.7	4794.4	4574.8	4747.7	4783.6

Tab. 3: Effect of crack depth on AE longitudinal wave speed.

Experiment number	Specimen 3				Specimen 4			
	v_1 ($m \cdot s^{-1}$)	v_2 ($m \cdot s^{-1}$)	v_3 ($m \cdot s^{-1}$)	v_4 ($m \cdot s^{-1}$)	v_1 ($m \cdot s^{-1}$)	v_2 ($m \cdot s^{-1}$)	v_3 ($m \cdot s^{-1}$)	v_4 ($m \cdot s^{-1}$)
1	4687.5	4545.5	4891.3	4838.7	4687.5	4545.5	4591.8	4838.7
2	4687.5	4545.5	4787.2	4761.9	4687.5	4687.5	4687.5	4838.7
3	4687.5	4545.5	4787.2	4761.9	4687.5	4545.5	4591.8	4838.7
4	4687.5	4545.5	4787.2	4761.9	5000.0	4545.5	4687.5	4838.7
5	4687.5	4545.5	4891.3	4838.7	4687.5	4545.5	4591.8	4838.7
6	4687.5	4545.5	4787.2	4761.9	5000.0	4545.5	4687.5	4838.7
7	4687.5	4545.5	4787.2	4761.9	5000.0	4545.5	4687.5	4838.7
8	4687.5	4545.5	4787.2	4761.9	4687.5	4545.5	4591.8	4838.7
9	4687.5	4545.5	4787.2	4761.9	4687.5	4687.5	4687.5	4761.9
10	4687.5	4545.5	4787.2	4761.9	5000.0	4545.5	4687.5	4838.7
Average value	4687.5	4545.5	4808.0	4777.3	4812.5	4573.9	4649.2	4831.0

Tab. 4: Effect of crack width on AE longitudinal wave speed.

Experiment number	Specimen 5				Specimen 6			
	v_1 ($m \cdot s^{-1}$)	v_2 ($m \cdot s^{-1}$)	v_3 ($m \cdot s^{-1}$)	v_4 ($m \cdot s^{-1}$)	v_1 ($m \cdot s^{-1}$)	v_2 ($m \cdot s^{-1}$)	v_3 ($m \cdot s^{-1}$)	v_4 ($m \cdot s^{-1}$)
1	5000.0	4687.5	4891.3	4615.4	5000.0	4545.5	4591.8	4838.7
2	4687.5	4545.5	4891.3	4615.4	4687.5	5000.0	4500.0	4761.9
3	4411.8	4285.7	4591.8	4838.7	5000.0	4285.7	4285.7	4838.7
4	5000.0	4166.7	4500.0	5000.0	4687.5	5000.0	4591.8	4761.9
5	4411.8	4166.7	4500.0	4615.4	4616.7	4285.7	4591.8	4761.9
6	5000.0	4166.7	4500.0	4615.4	5000.0	5172.4	4500.0	4838.7
7	5000.0	4285.7	4591.8	4615.4	5000.0	4545.5	4285.7	4838.7
8	4687.5	4545.5	4891.3	4615.4	4687.5	5000.0	4591.8	4761.9
9	5000.0	4687.5	4891.3	4838.7	4687.5	4545.5	4591.8	4761.9
10	4687.5	4545.5	4891.3	4615.4	5000.0	5172.4	4285.7	4838.7
Average value	4788.6	4408.3	4714.0	4698.5	4798.3	4755.3	4481.6	4800.3

From the above Tabs. 2, 3 and 4, the AE longitudinal wave speed of the crack-free specimen fluctuates after the crack is produced, and there is no obvious change with the change of crack size and distribution. To characterize the variation of the AE longitudinal wave speed, the speed decay rate η ($\eta = v_i - v/ v$, $i = 1,2,3,4$) was calculated based on the crack-free specimen 1, the calculation results are shown in Tab. 5, where S is the crack cross-sectional area and $\Delta\eta$ (η_{min} - η_{max}) is the rate of change difference. Comparing the test data of two specimens in Tab. 2, in the 10 independent tests of specimen 1, the AE longitudinal wave speed was 4838.7 $m \cdot s^{-1}$ and after making cracks on the surface of specimen 2, the AE longitudinal wave speed were all unstable without changing the size of the cracks, which is smaller than the longitudinal wave propagation speed on specimen 1, as shown in Tab. 5, with the AE longitudinal wave speed attenuation range of 5.45% ~ 0.92%. And with the increase of crack number, the linear relationship between AE longitudinal wave speed and the crack number is not obvious. Refraction, reflection, and transmission occur during the propagation of longitudinal waves (Ding et al. 2016, 2017), and this is exacerbated after the appearance of cracks, leading to fluctuations in the collected AE signal, which affects the stability of the propagation speed. In Tab. 3, only the crack depth was changed in the two specimens and the other conditions remained the same, and the crack depth increased by 2 mm in specimen 4 compared with specimen 3. From the test data, the AE longitudinal wave speed of the 10 independent tests were in fluctuation, and the difference between the two groups of test data was not too obvious. According to the analysis in Tab. 5, the variation range of AE longitudinal wave speed in specimen 3 and specimen 4 is close. It means that once the crack reaches a certain depth, the effect on the AE longitudinal wave speed was less significant. This is because the longitudinal wave undergoes a solid-gas-solid medium transformation at the crack boundary during the forward propagation, which causes the result that a certain degree of attenuation appears in the AE longitudinal wave speed. Since the crack width is not changed and the distance of longitudinal wave propagation in the air is not varied, its speed decay will stay within a certain range. As shown in Tab. 5, with the increase of crack cross-sectional area, the speed decay rate is all within 9%, while the difference of speed change rate is all within 8%.

To further investigate the effect of crack width on AE longitudinal wave speed, the crack widths of specimens 5 and 6 are changed (Tab. 4). Compared with the changes of crack depth and number, the speed fluctuation is more obvious, and the speed variation range is larger, with the speed variation ranges of 8.90% ~ 1.04% and 7.38% ~ 0.79%, respectively. It is shown that the effect of the variation of crack width on the AE longitudinal wave speed is more obvious, which is due to the increase of the crack width and thus the increase of the longitudinal wave propagation distance in the air medium, resulting in a more significant loss of the longitudinal speed and an increase of its speed instability.

Tab. 5: AE longitudinal speed decay rates at different cross-sectional areas.

Specimens number	S (mm^2)	$\eta_{min} \sim \eta_{max}$	$\Delta\eta$
Specimens 2	24	5.45% ~ 0.92%	4.53%
Specimens 3	36	6.06% ~ 0.63%	5.43%
Specimens 4	48	5.47% ~ 0.16%	5.31%
Specimens 5	64	8.90% ~ 1.04%	7.86%
Specimens 6	80	7.38% ~ 0.79%	6.59%

Different crack sizes and distributions all make a difference on longitudinal wave propagation (Tab. 5). On the one hand, because the wood itself belongs to heterogeneous materials, the density of the local area is different, and after the artificial production of cracks, the original structure is destroyed, therefore, the original density distribution in local areas of the wood is changed, and resulting in speed fluctuations. On the other hand, due to the generation of cracks, the boundary effect of AE signal in the propagation process is enhanced, the reflection of stress waves at the crack boundary in the direction of the wood along the grain is enhanced, and the difference of speed change rate increases with the increase of crack cross-sectional area.

Effect of crack on AE longitudinal wave energy

In the literature (Ming et al. 2021), it was shown that the AE signal longitudinal and transverse waves propagated in wood showed significant exponential attenuation, and the attenuation gradually became slower with the increase of propagation distance. To investigate the effect of crack variation on the AE longitudinal wave energy, the signal generator was used to generate a fixed frequency pulse train at the left end face, as shown in

Fig. 1. The AE signal from the broken lead core has a limited energy source and short duration, and decays rapidly in the wood, so a standard pulse signal was used as the AE source to calculate the AE longitudinal wave energy. In the literature (EI-Hadad et al. 2018), the researchers used signal generators as AE sources to output different frequency bands of pulsed signals to study the attenuation of different frequency bands of signals in wood. Since the resonant frequency of the AE sensor is 150 kHz, to generate a more stable AE source, the output pulse frequency of the signal generator was also set to 150 kHz, and the length of the pulse string was 15000 to ensure that each sensor can receive the pulse signal from the AE source. The AE signal collected in the experiment was amplified by a 40 dB preamplifier, so it needed to be reduced to the real AE signal, and then calculated the AE energy of each sensor according to Eq. 2, the unit is μJ.

To study the energy attenuation of AE longitudinal wave in different specimens, this test was performed by keeping the sensor and AE source positions constant. By changing the voltage level of the issued signal, the initial energy issued by the AE source was changed, the voltage level was set to 20 V, 15 V, 10 V, 5 V. So, the energy decay of different cracks can be studied corresponding to different amplitude conditions. To reflect the energy attenuation of each specimen at different amplitudes more intuitively, Fig. 4 shows the longitudinal wave energy decay curves of six specimens at different source voltages. Since the AE energy decays too fast in the wood, the true energy is taken as the vertical coordinate after the logarithm.

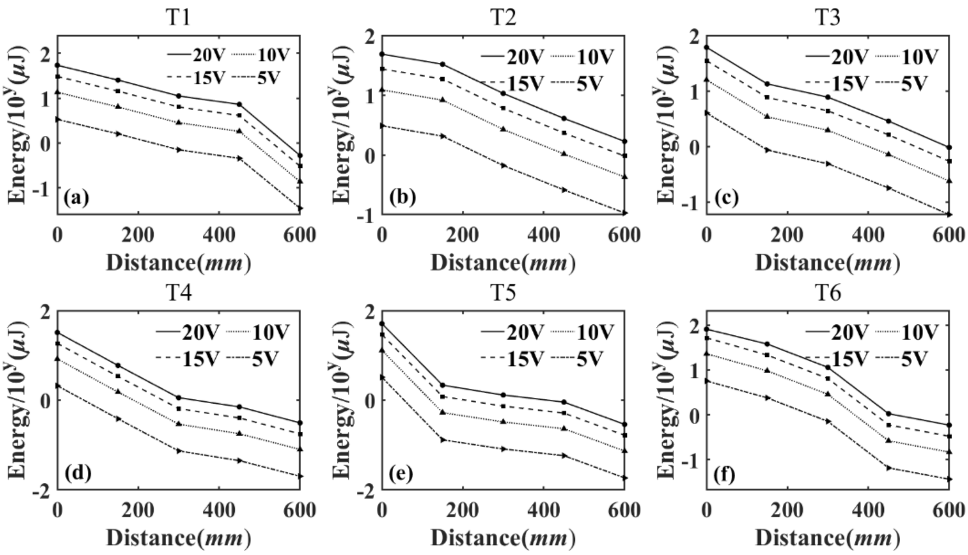

Fig. 4: Longitudinal wave energy attenuation curves of six specimens at different source voltages.

In Fig. 4a-f are the AE longitudinal wave energy attenuation curves of different source voltage levels corresponding to specimen 1 to specimen 6. All specimens show the same decay pattern when the source voltage level is changed, which indicates that the presence of cracks in the specimens or the change of the source voltage level did not affect the AE longitudinal wave energy attenuation law. However, it can be seen from Fig. 4 that the AE longitudinal wave energy decay rates are different in different specimens, while the corresponding energy decay rates of the same specimen are consistent, therefore, the energy decay rate of AE longitudinal wave can be used to characterize the influence of different cracks with energy decay. The energy data are linearly fitted to obtain the energy decay rate of each specimen (Fig. 5)

Fig. 5 shows the fitted energy decay curves of each specimen at different voltage levels, which characterizes the energy decay of different specimens. In the fitting process, the longitudinal wave energy measured by the S1 sensor closest to the AE source is regarded as 1, and then the energy measured by the other position sensors is normalized to obtain the fitting curve. In the fitting equation shown in Fig. 5, the x-front coefficient is the AE longitudinal wave attenuation coefficient at different voltage levels and its average value is taken, which is called the attenuation rate of the specimen and expressed as *K*. The larger the absolute value of *K* means, the faster the decay rate of AE longitudinal wave energy, and the *K* values of different specimens, which is shown in different specimens are shown in Tab. 6. To clarify the variation of the corresponding attenuation distances at different attenuation rates, the distances that can be reached by 50% and 90% attenuation of the AE longitudinal wave energy are used to quantify the characterization.

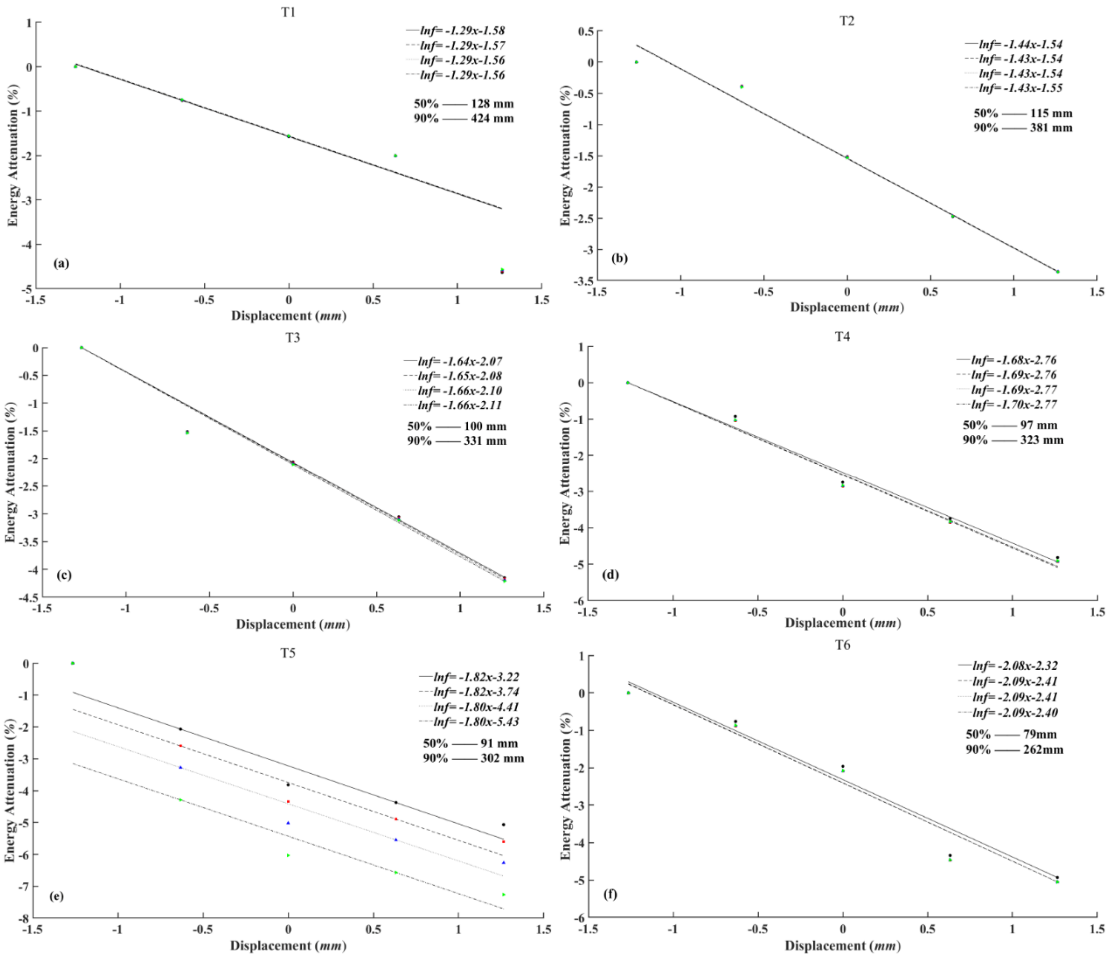

Fig. 5: Fitting curve of AE longitudinal wave energy attenuation.

In the calculation of AE longitudinal wave energy, due to the small distance and large energy value, there is still a significant difference in the order of magnitude between the energy value after taking the logarithm and the value of the distance, and the direct fitting is easily to produce large fitting errors, so the following centered linear treatment of the true distance is performed.

$$x = \frac{D - mean(D)}{std(D)} \quad (3)$$

where: D - the actual distance at which the AE sensor is placed, D∈[0,600 mm], when the sensor S1 is used as the origin position, x - the equivalent distance after transformation, namely the horizontal axis coordinate in Fig. 5, *mean*(D) - the expectation of D, and *std*(D) – the variance of D.

In this paper, the expectation and variance are 300 mm and 173.64 mm, respectively. The attenuation law of the AE longitudinal wave of six specimens with the change of equivalent distance x is shown in Eq. 4:

$$E_i = e^{Kx+b} \quad (4)$$

Substituting Eq. 3 into Eq. 4, the attenuation function of the AE wave energy with the actual distance D of different crack conditions is obtained (Eq. 5). All the variable parameters are shown in Tab. 6.

$$E_{Ti} = \alpha e^{\beta D} \quad (5)$$

Tab. 6: Variation of parameters corresponding to different cross-sectional areas of cracks.

Parameters \ Specimens	1	2	3	4	5	6
S (mm^2)	0	24	36	48	64	80
K	-1.29	-1.43	-1.65	-1.69	-1.81	-2.08
b	-1.57	-1.54	-2.09	-2.77	-4.20	-2.39
α	1.9234	2.5361	2.1398	1.1616	0.342	3.3322
β	-0.0074	-0.0082	-0.0095	-0.0097	-0.0104	-0.012

Combined with the analysis in Fig. 5 and Tab. 6, the energy decay rate of the pulse string signal on the crack-free specimen 1 is 1.29, and the distances traveled for 50% and 90% energy decay are 128 mm and 424 mm, respectively. With the increase of crack cross-sectional area, the energy decay rate also increases gradually, and the maximum increase rate is 61% based on crack-free specimens. The propagation distance is gradually shortened, and the distances of 50% and 90% energy attenuation are shortened from 128 mm and 424 mm to 79 mm and 262 mm, respectively. It can be characterized that the change of crack size influences its longitudinal wave energy, and this effect is gradually aggravated with the increase of the crack size. This is because longitudinal waves can propagate in solid, liquid and gaseous media, and the acoustic impedance of different media is different, resulting in different degrees of energy loss in different media propagation. The acoustic impedance of air medium is 4.3×10^{-4} kg/(m^2.s), and the propagation speed of longitudinal wave in air is 340 m$\cdot$s^{-1}, which is much smaller than the propagation speed in wood. Therefore, in the crack-free specimen 1, AE signals propagated mainly inside the wood, and the longitudinal wave energy loss is less compared to that in air, so the propagation distance is longer and the attenuation rate is smaller. However, after the crack is generated, the longitudinal wave propagates through the crack boundary in the air, resulting in a large energy loss and a shortened propagation distance.

Comparing Fig. 5a and 5b, the longitudinal wave propagation distance appears to be significantly reduced after crack generation and the attenuation rate appears to be significantly increased, and the effect of cracks on longitudinal wave energy begins to appear. When other conditions remain unchanged, the propagation distance and energy attenuation rate do not change significantly by changing the crack depth of the specimen (Figs. 5c,d). It shows that the variation of crack depth also has no significant effect on the longitudinal wave energy. Because the change in crack depth does not change the propagation distance of the longitudinal wave in the air, there is little difference in the energy lost in the air medium, and the energy decay rate is very close. Figs. 5e,f are the fitting curves under the change of crack width, the attenuation distance in the two figures showed a significant difference, and the energy attenuation rate also increased significantly, compared with the change of other conditions, the energy attenuation is more obvious. This is because the increase of crack width leads to the increase of propagation distance in the air, which further aggravates the attenuation of longitudinal wave energy.

From the attenuation distance in Fig. 5, it takes a shorter distance for the AE longitudinal wave energy to decay to 50% compared to the subsequent 40% increase in energy, indicating that the longitudinal wave energy decays faster in the early stage of propagation, and the subsequent attenuation gradually slows down. This is because the AE signal is mainly composed of high-frequency components when propagating in the previous stage, high-frequency components contain large energy and the attenuation is more obvious. However, the AE signal can form stable standing waves during propagation, which carries less energy and does not propagate forward but can be affected by the wood itself, so it will be gradually decay at its vibration position. It can be shown that AE energy attenuation mainly occurs at the early stage of propagation, while the attenuation at the later stage is mainly dominated by standing waves' attenuation. The results of this research are consistent with those of EI-Hadad et al. (2018), Ming et al. (2021) and Ding et al. (2022), indicating that the energy decay pattern of the AE signals in different wood materials is also the same, which is consistent with exponential decay, and the energy decay is fast in the early stage and slower in the later stage. At the same time, the proposed energy attenuation effective distance can provide the basis for the arrangement of wood AE sensors and the effective extraction of AE signals. This is consistent with the research conclusion of Li et al. (2020) in concrete, which provides reference for AE source localization research.

CONCLUSIONS

Based on the mechanical wave vibration theory, the longitudinal wave analysis experiment was conducted to study the propagation speed and energy attenuation of longitudinal waves under different cracked specimens using lead core fracture and signal generator as the simulated AE source. The effects of different crack types on longitudinal wave energy and propagation speed were explored. It was found that the change of longitudinal wave energy was more obvious than that of propagation speed. The speed of the AE longitudinal wave was calculated based on TDOA, and the propagation speed of the longitudinal wave in the crack-free specimen is 4838.7 $m \cdot s^{-1}$. After the crack was created, the speed all showed a tendency to decay, and the speed loss was within 9%. The change of crack width has a more obvious influence on speed than that of other conditions. When the crack width was 8 mm and 10 mm, the attenuation range of longitudinal wave speed was 8.9% ~ 1.04% and 7.38% ~ 0.79%, respectively. The longitudinal wave speed has a certain degree of loss and fluctuation, which is due to the artificial crack's generation, on the one hand, the original structure of the wood specimen is destroyed, and the density distribution of the wood is changed. On the other hand, the crack enhances the boundary effect of the AE signal, thereby increasing the reflection of the stress wave at the crack boundary along the grain direction of wood, which leads to fluctuations and attenuation of the longitudinal wave speed.

By using the signal generator as a simulated AE source, the effect of cracks on the attenuation of longitudinal wave energy was studied, and the voltage level of the generated signal was adjusted to change its initial energy value without changing the location of the AE source. The change of crack and voltage level did not affect the longitudinal wave energy decay law, but the energy decay rate and propagation distance were different. In the crack-free specimen, the longitudinal wave energy decay rate was 1.29, and the distances for 50% and 90% decay were 128 mm and 424 mm, respectively. After the crack was created, the decay rates all showed a significant increase, with a maximum increase of 61%, the propagation distances showed a significant decrease, and the energy attenuation distances of 50% and 90% were reduced to 79 mm and 262 mm compared with those of the crack-free specimen. Since the longitudinal wave can be propagated in any medium, and the acoustic impedance is the largest when propagating in air, the energy loss is larger, so when the crack width increases, the longitudinal wave energy decays faster and the propagation distance is smaller. Regardless of the existence of cracks in the specimen, the longitudinal wave energy decays faster before 50%, and the decay slows down during the subsequent propagation.

This study explored the influence of wood cracks on the propagation speed and energy of acoustic emission longitudinal waves and did not explore the influence of different type of cracks on longitudinal wave propagation. Meanwhile, the crack identification and localization study can be conducted based on the variation of longitudinal wave energy and speed in subsequent studies.

ACKNOWLEDGMENTS

The authors are grateful to the National Natural Science Foundation of China (NO: 32160345, NO: 31760182) for funding this research. Startup fund for introducing talents and scientific research of Anhui University of Engineering (NO: 2021YQQ037)

REFERENCES

1. Aljets, D., Chong, A., Wilcox, S., Holford, K., 2012: Acoustic emission source location on large plate-like structures using a local triangular sensor array. Mechanical Systems and Signal Processing 30: 91-102.
2. Azadi, M., Alizadeh, M., Jafari, S.M., Farrokhabadi, A., 2021: Cumulative acoustic emission energy for damage detection in composites reinforced by carbon fibers within low-cycle fatigue regime at various displacement amplitudes and rates. Polymers and Polymer Composites 29(9): S36-S48.
3. Bertolin, C., Ferri, L.D., Razavi, M.J., Berto, F., 2020: Acoustic emission NDT for monitoring hygro-mechanical reactions of coated pine wood: a methodological approach. Procedia Structural Integrity 28: 208-217.
4. Deng, T., Ju, S., Wang, M., Li, M., 2021: Study on propagation law of acoustic emission signals on anisotropic wood surface. Wood Research 66(4): 517-527.
5. Diakhate, M., Bastidas-Arteaga, E., Pitti, R.M., Schoefs, F., 2017: Cluster analysis of acoustic emission activity within wood material: Towards a real-time monitoring of crack tip propagation. Engineering Fracture Mechanics 180: 254-267.
6. Ding, J.C., Wu, B., He, C.F., Zhou, Y.F., 2016: Reflection and transmission of longitudinal wave in the adhesive structure with different interface forms. Journal of Huazhong University of Science and Technology (Nature Science Edition) 44(6): 84-90.
7. Ding, J.C., Wu, B., He, C.F., 2017: Propagation of longitudinal wave in adhesive structure with linear viscous adhesive layer. Acta Materiae Compositae Sinica 34(8): 1801-1809.
8. Ding, R., Fang, S.Y., Luo, R.H., Lai, F., Yang, Z.L., Huang, C.L., Li, M., 2022: Propagation characteristics and energy attenuation law of surface shear waves and internal longitudinal waves in Mongolian scotch pine sawn timber based on acoustic emission. Chinese Journal of Wood Science and Technology 36(01): 36-42.
9. Dong, H.P., Li, M., 2020: Wood acoustic emission event identification based on instantaneous frequency and damage monitor. Journal of Northwest Forestry University 35(02): 229-234.
10. Dong, L., Hu, Q., Tong, X., Liu, Y., 2020: Speed-free MS/AE source location method for three-dimensional hole-containing structures. Engineering 6(7): 827-834.
11. El-Hadad, A., Brodie, G.I., Ahmed, B.S., 2018: The effect of wood condition on sound wave propagation. Open Journal of Acoustics 8(3): 37-51.
12. Fang, S.Y., Qiu, R.Z., Li, Ming., 2018: Wood AE signal features based on improved EMD algorithm. Journal of Vibration and Shock 37(23): 292-298
13. Guo, Y., Zhu, S., Chen, Y., Liu, D., Li, D., 2019: Acoustic emission-based study to characterize the crack initiation point of wood fiber/HDPE composites. Polymers 11(4): 701.
14. Ju, S., Li, X.C., Luo, T.F., Li, M., 2019: Propagation characteristics and energy attenuation law of surface shear waves and internal longitudinal waves in Mongolian scotch pine sawn timber based on acoustic emission. Chinese Journal of Wood Science and Technology 4(02): 48-53.

15. Kowalski, S.J., Molinski, W., Musielak, G., 2004: The identification of fracture in dried wood based on theoretical modelling and acoustic emission. Wood Science & Technology 38(1): 35-52.
16. Lamy, F., Takarli, M., Angellier, N., Dubois, F., Pop, O., 2015: Acoustic emission technique for fracture analysis in wood materials. International Journal of Fracture 192(1): 57-70.
17. Li, D., Yang, K., He, Z., Zhou, H., Li, J., 2020: Acoustic emission wave speed attenuation of concrete and its application in crack localization. Sustainability 12(18): 7405.
18. Li, Y., Luo, T.F., Yu, S.S., Shen, L.J., Li, M., 2017: Signal propagation characteristics of acoustic emission and Douglas fir glulam beams. Journal of Northwest Forestry University 32(05): 197-201+251.
19. Liu, B., Khvesyuk, V. I., 2020: Analytical model for thermal boundary conductance based on elastic wave theory. International Journal of Heat and Mass Transfer 159: 120117.
20. Liu, X.L., Liu, Z., Li, X.B., Rao, M., Dong, L.J., 2018: Wavelet threshold de-noising of rock acoustic emission signals subjected to dynamic loads. Journal of Geophysics and Engineering 15(4): 1160-1170.
21. Lukomski, M., Strojecki, M., Pretzel, B., Blades, N., Beltran, V.L., Freeman, A., 2017: Acoustic emission monitoring of micro-damage in wooden art objects to assess climate management strategies. Insight - Non-Destructive Testing and Condition Monitoring 59(5): 256-264.
22. Ming, L., Minghua, W., Rui, D., Tingting, D., Saiyin, F., Fei, L., Ruihan, L., 2021: Study of acoustic emission propagation characteristics and energy attenuation of surface transverse wave and internal longitudinal wave of wood. Wood Science and Technology 55(6): 1619-1637.
23. Ohtsu., Masayasu., 2016: Elastic wave methods for nde in concrete based on generalized theory of acoustic emission. Construction and Building Materials 122: 845-854.
24. Raczkowski, J., Lutomski, K., Moliński, W., Wo, R., 1999: Detection of early stages of wood decay by acoustic emission technique. Wood Science & Technology 33(5): 353-358.
25. Reiterer, A., Sinn, G., Stanzl-Tschegg, S.E., 2002: Fracture characteristics of different wood species under mode I loading perpendicular to the grain. Materials Science & Engineering A 332(1-2): 29-36.
26. Rescalvo, F.J., Rodríguez, M., Bravo, R., Abarkane, C., Gallego, A., 2020: Acoustic emission and numerical analysis of pine beams retrofitted with FRP and poplar Wood. Materials 13(2): 435.
27. Ritschel, Zhou, Brunner, A.J., Fillbrandt, Niemz, 2014: Acoustic emission analysis of industrial plywood materials exposed to destructive tensile load. Wood Science and Technology 48(3): 611-631.
28. Sause, M.G.R., 2011: Investigation of pencil-lead breaks as acoustic emission sources. Journal of Acoustic Emission 29: 184-196.
29. Shen, K.N., Zhao, H.L., Ding, X.Z., Li, M., 2015: Wavelet analysis of acoustic emission signal in wood damage and fracture process. Journal of Henan University of Science & Technology (Natural Science) 36(03): 33-37+36.

30. Ting, T., 2006: Longitudinal and transverse waves in anisotropic elastic materials. Acta Mechanica 185(3-4): 147-164.
31. Urbaha, M., Agafonovs, I., Turko, V., Feuks, J., Korhs, J., 2021: Acoustic emission monitoring of composite specimens with impact damage during static compression test. IOP Conference Series. Materials Science and Engineering 1140(1): 012001-012008.
32. Vinogradov, A.Y., Merson, D.L., 2018: The nature of acoustic emission during deformation processes in metallic materials. Low Temperature Physics 44(9): 930-937.
33. Vun, R., Dehoop, C., Beall, F., 2005: Monitoring critical defects of creep rupture in oriented strandboard using acoustic emission: incorporation of EN 300 standard. Wood Science & Technology 39(3): 199-214.
34. Wang, M.H., Deng, T.T., Ju, S., Li, C.X., Li, X.S., Li, M., 2020: Effect of wood surface crack on acoustic emission signal propagation characteristics. Journal of Northeast Forestry University 48(10): 82-88.
35. Wang, M.H., Deng, T.T., Fang, S.Y., Li, X.S., Lai, F., Li, M., 2021: Generation and characteristics of simulated acoustic emission source of wood. Journal of Northeast Forestry University 49(06): 96-101+118.
36. Wu, Y., Shan, Z.P., Wang, F., Tian, G.L., 2014: Acoustic emission characteristics and felicity effect of wood fracture perpendicular to the grain. Journal of Tropical Forest Science 26(4): 522-531.
37. Xing, Y., Zhang, G., Wan, B., Zhao, H., 2019: Subcritical fracturing of sandstone characterized by the acoustic emission energy. Rock Mechanics and Rock Engineering 52(7): 2459-2469.

CHANGLIN HUANG, SAIYIN FANG, YUE ZHAO, FEILONG MAO, ZHOULING YANG, TINGTING DENG
SOUTHWEST FORESTRY UNIVERSITY
SCHOOL OF MACHINERY AND TRANSPORTATION ENGINEERING
KUNMING 650224
CHINA

MING LI[1,2]*
ANHUI POLYTECHNIC UNIVERSITY
[1]KEY LABORATORY OF ADVANCED PERCEPTION AND INTELLIGENT CONTROL OF HIGH-END EQUIPMENT OF MINISTRY OF EDUCATION
ANHUI 241000, CHINA
[2]SCHOOL OF ELECTRICAL ENGINEERING
ANHUI 241000, CHINA
*Corresponding author: swfu_lm@swfu.edu.cn